Article

Synergetic effect of a surfactant on the facile fabrication and high detectivity of an inverted organic bulk heterojunction photodiode

Jae Un Ha, Kyounghwan Kim, Seongwon Yoon, Kyu Min Sim, Jangwhan Cho, and Dae Sung Chung

ACS Photonics, **Just Accepted Manuscript** • DOI: 10.1021/acsphotonics.7b00607 • Publication Date (Web): 31 Jul 2017

Synergetic effect of a surfactant on the facile fabrication and high detectivity of an inverted organic bulk heterojunction photodiode

Jae Un Ha[†]*, Kyounghwan Kim*[†]*, Seongwon Yoon*[†]*, Kyu Min Sim*[†]*, Jangwhan Cho*[†] *and Dae Sung Chung*[†]*

[†] Department of Energy Systems Engineering, Daegu Gyeongbuk Institute of Science and Technology (DGIST), Daegu 42988, Republic of Korea

Abstract

A new photodiode fabrication strategy for organic photodiodes is proposed, involving the use of small amount of cationic surfactant to a blend solution aiming synergetic effects of facile device fabrication and high performances. By adding small amount of cationic surfactant (Cetyl trimethylammonium bromide (CTAB)) to a blend solution consisting of poly(3-hexylthiophene) (P3HT) and phenyl-C61-butyric acid methyl ester ($PC_{60}BM$), indium tin oxide (ITO) work function can be reduced to ~4.55 eV due to the formation of CTAB dipole layer, without the insertion of oxide buffer layers. Furthermore, we observe a meaningful contribution of the addition of CTAB to the morphology of the active layer in terms of the inter-miscibility between P3HT and $PC_{60}BM$. Various photophysical, morphological and structural analyses provided strong evidences for the enhanced inter-miscibility between P3HT and $PC_{60}BM$. Owing to the synergetic contribution of CTAB, the resulting photodiode with inverted diode geometry reveal high detectivity of $\sim 2.5 \times 10^{12}$ Jones based on a low dark current of 1.3×10^{-8} A/cm^2 at −1 V. In addition, a high −3 dB frequency of 4 kHz and a linear dynamic range of 100 dB are demonstrated. This work opens the possibility of facile and simple photodiode patterning/printing processes.

KEYWORDS

work function tuning, organic photodiode, work function, low dark current, high-detectivity

Introduction

Organic photodiode is an emerging research theme with potential applications as image sensor devices to replace Si photodiodes.[1-3] An organic photodiode can be featured as an organic active layer, consisting of the heterojunction between the electron donor and electron acceptor organic semiconductors. The major advantage of organic semiconductors versus silicon for photodiode application is the possibility of forming thin films of the active layer because of their high absorption coefficients.[4,5] Organic semiconductors can absorb most of the incident photons of visible light within a thickness of only several hundreds of nanometers, whereas Si requires thickness of several micrometers for a similar absorption.[4-7] Therefore, when a photodiode is composed of organic semiconductors, the light path is shortened remarkably. More importantly, cross-talk between pixels can be prevented, which ultimately improves the integration degree of the image sensor pixels.[4,8-10] In addition, solution processes, which are possible when using organic semiconductors, have commercial value, allowing the manufacture of image sensors at a lower cost and improving the compatibility with plastic substrates.[11-13]

Since the pioneering works conducted by Gong et al.,[14] significant research efforts have been made to realize high-performance organic photodiodes. The most important figure-of-merit of the photodiode is the signal-to-noise ratio because of its sensor applications. The most widely accepted signal-to-noise parameter for photodiodes is the specific detectivity (D*), which has units of Jones:[15]

$$\boldsymbol{D^* = \frac{e\lambda\sqrt{A}\cdot EQE}{hci_n}}$$

where e is the elementary charge, λ is the wavelength of incident light, A is the area of the active layer, EQE is the external quantum efficiency, h is Planck's constant, c is the speed of

light, and i_n is the noise current level. Measuring D^* enables the direct comparison of photodiode performance between different devices by normalizing the device area. From the equation, one can see that both high quantum efficiency and low noise current are essential for high detectivity. Therefore, most research efforts on OPDs have also focused on these targets. Various interlayers have been designed as blocking layers for holes and electrons to reduce the noise current.[16,17] However, the introduction of these additional blocking layers accompany complicated fabrication step as well as interface issues, which is not feasible for solution-based patterning processes. For achieving high quantum efficiency, the overall idea is basically the same for organic photovoltaics (OPVs) because OPDs and OPVs have the same device structure. The choice of solvent, additive, and post-annealing step exerts dramatic effects on the morphology of the BHJ film and, thus, on the quantum efficiency of OPVs.[18-20] However, there is a very important difference between an OPD and OPV: an OPD requires a much thicker active layer than does an OPV, mainly to maintain a low noise current.[3,21] Therefore, from the viewpoint of EQEs, the photodiode has different research requirements from those of OPVs.

In this study, we report a new and facile method to realize high quantum efficiencies and low noise currents in inverted photodiodes by introducing surfactant. An inverted photodiode is beneficial for stable OPD operation by replacing the PEDOT:PSS mixture with more air-stable inorganic semiconductors such as ZnO and TiO_2. Here, we propose the use of a cationic surfactant as an additive of the BHJ blend of the inverted OPD. This is 1) to fundamentally exclude the use of the ZnO/TiO_2 interlayer, which requires toxic and high-temperature manufacturing processes as well as an undesirable organic/inorganic interface, and 2) to optimize the morphology of the active layer of the OPDs, which should be sufficiently thick (~700 nm) for low noise current. We show that the addition of a cationic surfactant into the BHJ blend

solution has synergetic effects: 1) the realization of the preferential adsorption of the cationic surfactant onto the indium tin oxide (ITO) surface, reducing the work function of ITO and allowing the exclusion of the ZnO/TiO_2 interlayer, and 2) the formation of a finer intermixed morphology between the donor and acceptor and thus high EQE even in thick active layer, which can be attributed to the surfactant-assisted enhanced miscibility.

Methods

Materials: poly(3-hexylthiophene) (P3HT) was purchased from RIEKE METALS, phenyl-C61-butyric acid methyl ester ($PC_{60}BM$) was purchased from Nano-C and Cetyltrimethylammonium bromide (CTAB) was purchased from Sigma-Aldrich. All the materials were used without further purification steps.

Photodiode fabrication: ITO-patterned glass substrates (sheet resistance of ~15 Ω/sq.) were mechanically cleaned with aqueous hydrochloric acid solution, followed by sequential sonications in Mucasol solution, deionized water, acetone, and isopropanol. Cleaned substrates were then dried in nitrogen-flow. Prior to film deposition, the substrates were cleaned with UV ozone for 10 min to remove the organic contaminants and increase the surface wettability. Ternary P3HT:$PC_{60}BM$:CTAB (1:0.7:0.09 in weight) blend solution was dissolved in chloroform at 30 mg/mL at 60˚C for 12h. The blend solution was spin-coated onto the UV ozone treated ITO substrate for over 300 s in N_2-filled glove box. Molybdenum(IV) trioxide (MoO_3) interlayer and Ag electrodes were sequentially deposited onto the active layer by using thermal evaporation under high vacuum.

Characterization: Dark and illuminated *J–V* characteristics were analyzed by LabView-controlled Keithley 2400 sourcemeter combined with Oriel Cornerstone 130 1/8 m monochromator. To measure LDR, two different light sources were used: A monochromatic light from a 150 W xenon arc lamp dispersed from the monochromator was used for light intensity below 47 μW/cm^2 and a laser diode (520 nm) modulated by AFG310 arbitrary function generator (Tektronix) at 30 Hz was used for light intensity up to 0.5 W/cm^2. All the light intensities were calibrated with an Si-photodetector. Bode plot was plotted with the combination of TDS5052

digital phosphor oscilloscope (Tektronix) and the laser mentioned above at the light intensity of 0.9 mW/cm^2. Noise current data were collected directly from the Stanford Research SR830 Lock-in Amplifier and measured noise currents were normalized by the input bandwidth. All measurements were performed in an N_2-filled glove box. The UPS and GIXD data were recorded at the 4D and 9A beam lines at the Pohang Accelerator Laboratory. The X-rays coming from the in-vacuum undulator (IVU) were monochromated (E = 11.06 keV) using Si(111) double crystals and then focused at the detector position using a K–B focusing mirror system. The horizontal and vertical beam sizes were 300 (H) μm and 30 (V) μm, respectively. The incidence angle (α_i) was adjusted to 0.13°, which is above the critical angle. GIXD patterns were recorded with a 2D CCD detector (Rayonix SX-165). The diffraction angles were calibrated using pre-calibrated sucrose (monoclinic, P21) and the sample-to-detector distance was approximately 225 mm. DSC curves were obtained by using DISCOVERY DSC (TA Instruments-Waters LLC). The powder samples of the nominal mass of 5 ± 0.5 mg were measured in alumina crucibles from 100 °C temperature to 330 °C under flowing nitrogen atmosphere at heating rates of 5 °C/min. Morphological images were obtained by using an atomic force microscope (Park systems, NX20).

Results and Discussion

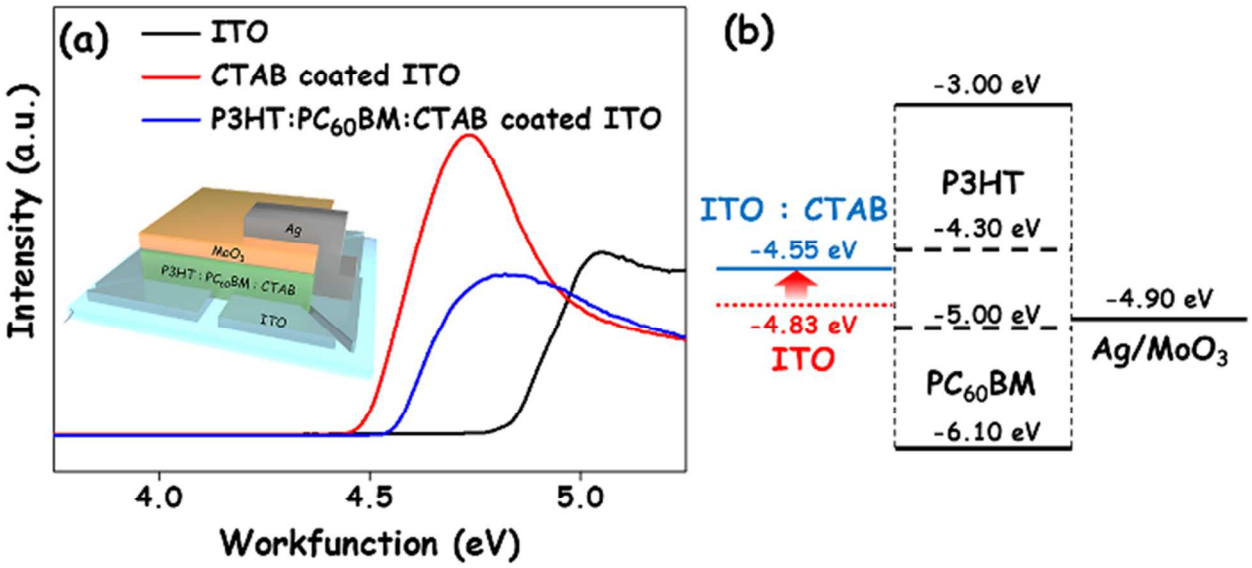

Figure 1 (a) The UPS spectra in secondary-cutoff region and (b) the energy band diagram of materials used in this report.

A schematic of the photodiode device structure is shown in the inset of Figure 1(a). A P3HT:$PC_{60}BM$:CTAB solution in chloroform was spin-coated onto pre-patterned ITO electrodes, forming a thick active layer (~700 nm). During the drying of the deposited solution, the cationic head group of the surfactant molecules is preferentially adsorbed onto the electron-rich ITO surface, so the hydrophobic tails mix with the organic semiconductor. Such a preferential adsorption of the ammonium groups of the CTAB cations onto the ITO surface results in the formation of a thin dipole (CTAB) layer between the ITO electrode and the active layer. Such a dipole direction, with alkyl chain heading to the semiconductor layer is known to reduce the work function of the metal electrode.[22] Figure 1(a) shows the UPS spectra obtained from pristine ITO, ITO/CTAB, and ITO/P3HT:$PC_{60}BM$:CTAB surfaces. In the case of ITO/P3HT:$PC_{60}BM$:CTAB, to see the work function shift of the ITO surface, we deposited a very thin layer (~10 nm) of P3HT:$PC_{60}BM$:CTAB onto the ITO surface. From the UPS spectra, the work function can be obtained from the secondary cut-off region. The obtained work

function of the ITO electrode with CTAB treatment was 4.48 eV, a decrease of ~0.35 eV from that of pristine ITO which can be attributed to the adsorption of CTAB dipole layer. In the case of the ITO electrode with an upper deposited layer of P3HT:$PC_{60}BM$:CTAB, the work function was ~4.55 eV, also a decrease of ~0.3 eV from that of pristine ITO. The difference between the ITO/CTAB and ITO/P3HT:$PC_{60}BM$:CTAB surfaces can be attributed to the lower adsorption density of CTAB molecules when mixed with other semiconductor materials, presumably resulting from a smaller free volume. Consequently, the ITO/P3HT:$PC_{60}BM$:CTAB/MoO_3/Ag diode structure works as an inverted diode, as indicated in Figure 1(b). This device architecture is much simpler than the case of a typical inverted diode of ITO/ZnO/active-layer/MoO_3/Ag, especially considering the complex/toxic fabrication procedure of the ZnO layer. In addition to modifying the work function of the electrode, the use of a surfactant can also have a positive role in improving the morphology of the photoactive layer. Thin films of P3HT and $PC_{60}BM$ have very different surface energies arising from their electron-deficient and electron-rich natures, respectively. When mixed with a small amount of CTAB before the formation of thin films, we found out that P3HT and $PC_{60}BM$ could possess closer surface energy values to each other. The surface energy of the thin P3HT film, which was originally 27.8 ± 0.6 mJ/m^2, increased to 31.5 ± 0.7 mJ/m^2 on the addition of CTAB to the casting solution, presumably due to the interaction between the hexyl chains of P3HT and the cetyl chains of CTAB, which exposes the polar groups of CTAB to the surface. At the same time, the thin $PC_{60}BM$ film, which had an original surface energy of 38 ± 0.8 mJ/m^2, decreased to 36.5 ± 0.5 mJ/m^2 on the addition of CTAB owing to the preferential surface arrangement of cetyl groups of CTAB. Therefore, when these three molecules are mixed to form a BHJ film, the miscibility of P3HT and $PC_{60}BM$ should be enhanced because of the surface-active behavior of CTAB. The role of such a surfactant

becomes important because a thick active layer is required to suppress the dark current in the OPD.[23,24]

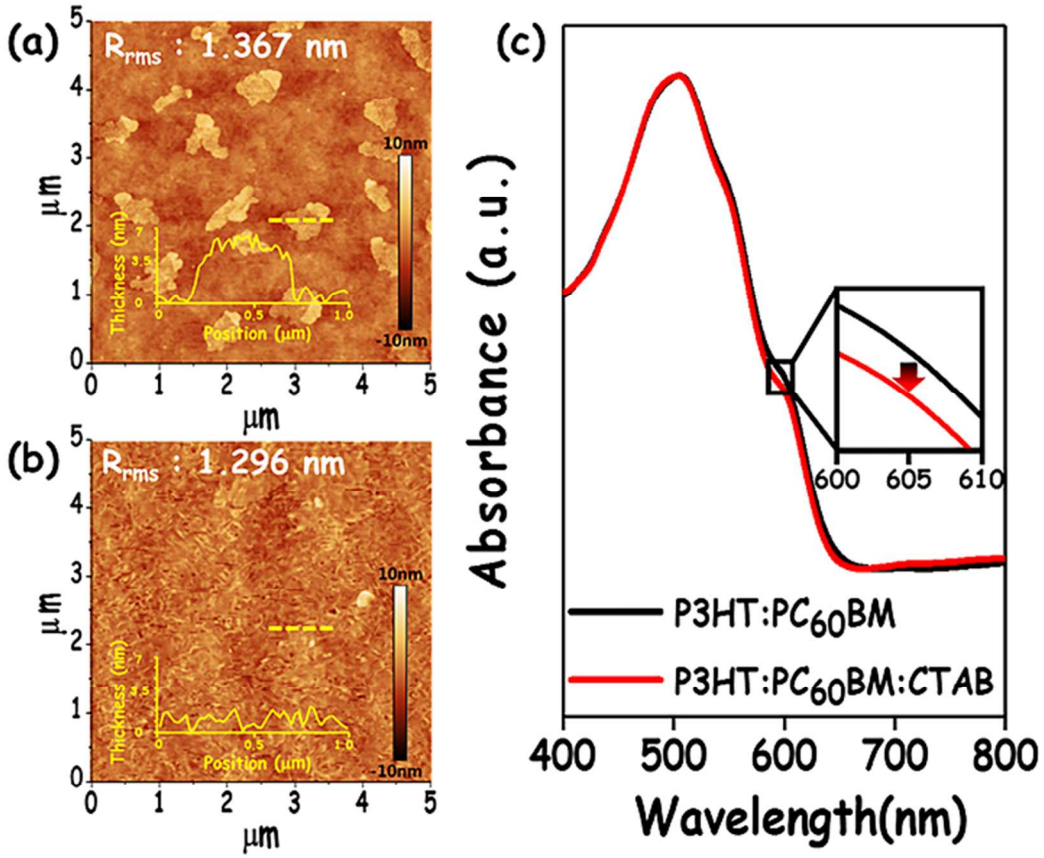

Figure 2 AFM topography images of (a) P3HT:PC_{60}BM mixture and (b) P3HT:PC_{60}BM:CTAB mixture films with thickness of ~700 nm. The inset graphs of (a) and (b) describe the thickness information of regions marked as dashed lines. (c) UV-vis absorption spectra of P3HT:PC_{60}BM mixture and P3HT:PC_{60}BM:CTAB mixture films.

As shown from the atomic force microscope (AFM) topography images in Figures 2(a) and 2(b), the thick (~700 nm) P3HT:PC_{60}BM BHJ film casted from chloroform has large (>1 μm in width) crystalline domains, which cannot be observed in the cases of conventional thin films (<200 nm) of an OPV prepared with an optimized deposition protocol. Interestingly, these large crystalline domains reduce in size and only small fibrillary domains remain after the addition of CTAB, which suggests that the formation of a smaller domain size in CTAB-added device could enhance the interfacial area in comparison to the CTAB-free case. Similar morphologies can be

found in other non-intercalating polymer BHJ systems with optimized post-treatments.[20] UV-Vis absorption spectra of the P3HT:$PC_{60}BM$ blend films without and with CTAB are presented in Figure 2(c). In general, three distinct absorption peaks or shoulders can be assigned to the π-π* transition (511 nm) and π-π stacking (555 and 605 nm) of P3HT molecules. After the addition of CTAB, the absorption shoulder near 605 nm decreased apparently, suggesting that the packing structure of P3HT was affected by the addition of CTAB.

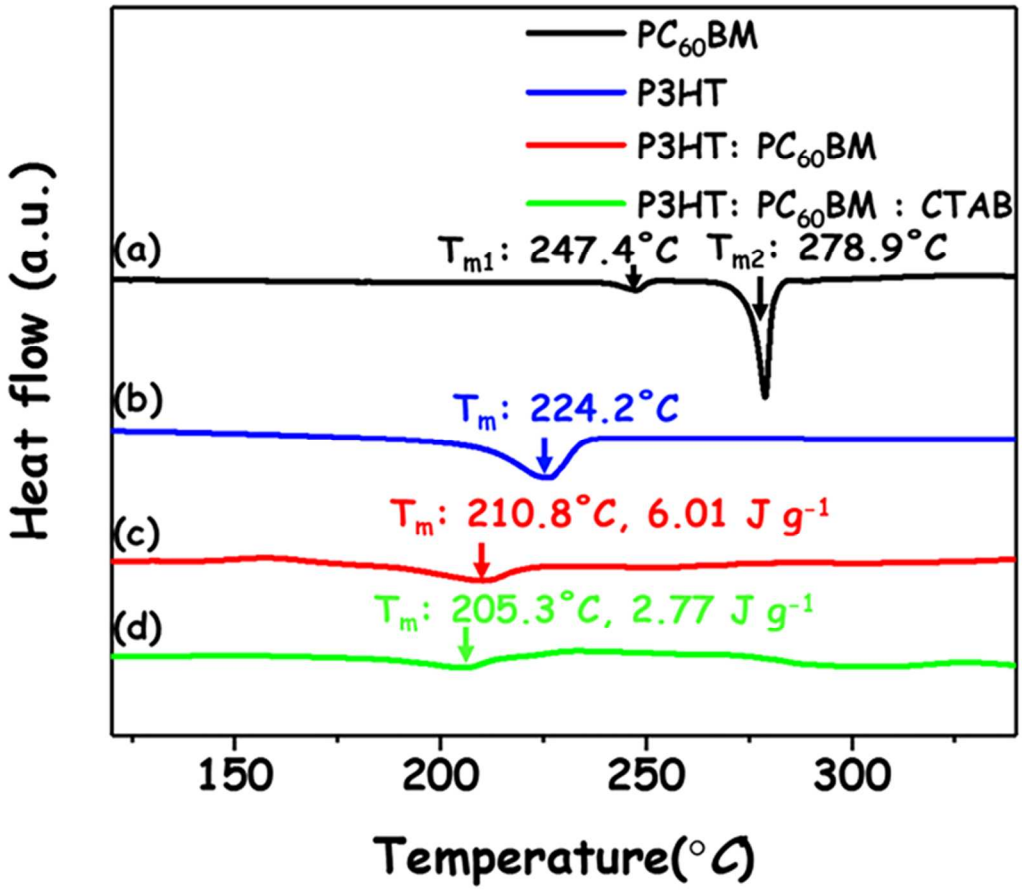

Figure 3 The DSC curves of (a) pristine PC60BM, (b) pristine P3HT, (c) P3HT:PC60BM mixture, and (d) P3HT:PC60BM:CTAB mixture. The heating rate of 5˚C/min was used under a nitrogen atmosphere.

As shown in Figure 3, Differential scanning calorimetry (DSC) measurements were performed to investigate the finer mixing of the P3HT:$PC_{60}BM$ blend on the addition of CTAB. DSC measurements were made for the pristine materials (P3HT and $PC_{60}BM$) and blend systems

(P3HT:$PC_{60}BM$ and P3HT:$PC_{60}BM$:CTAB) under the same thermal pretreatment conditions as those of device fabrication with a scan speed of 5 °C/min for both heating and cooling. As summarized in Figure 3, pristine films had distinct melting temperatures ($T_{m,P3HT}$:224.2 °C), ($T_{m1,PC60BM}$:247.4˚C) and ($T_{m2,PC60BM}$:278.9 °C), respectively. It is well known that higher inter-miscibility makes T_m of the blend system shift to a lower temperature with lower peak intensity and smoother shape in DSC.[25] In the case of the P3HT:$PC_{60}BM$ blend system, the corresponding T_m value was clearly observed at 210.8 °C with the enthalpy change of 6.01 J/g, although they were slightly shifted to lower temperature compared to those of both original materials. Interestingly, in the case of ternary P3HT:$PC_{60}BM$:CTAB blend, the DSC melting peak became almost featureless with the enthalpy change of only 2.77 J/g and the peak position was also further shifted to lower temperature (205.3 °C). These data give more solid evidence that the addition of CTAB improves the intermixing of P3HT and $PC_{60}BM$.

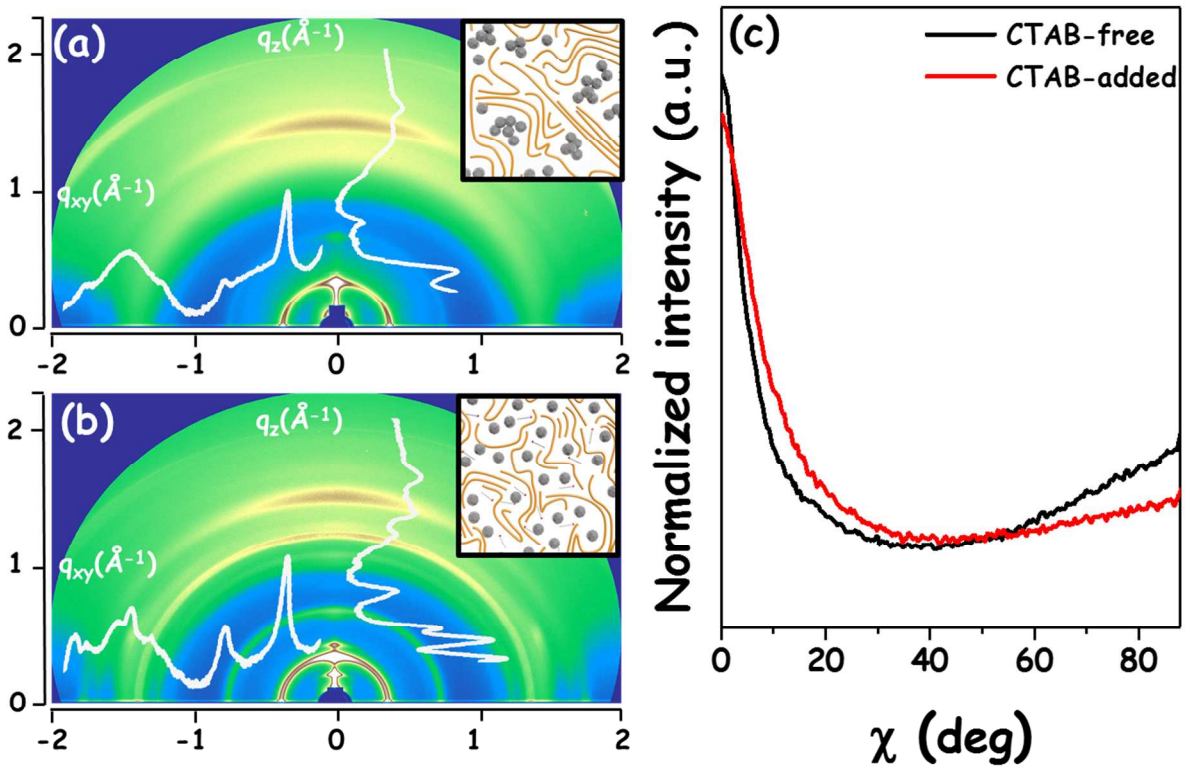

Figure 4 The 2D-GIXD patterns for (a) CTAB-free and (b) CTAB-added thin films and their extracted corresponding profiles along with q_z and q_{xy} axes. The insets show schematic crystalline structures of donor/acceptor blends estimated from GIXD study. (c) The extracted pole-figure profiles for both films. The details of pole-figure can be found in the text.

2D-GIXD measurement and analyses were conducted to investigate the effect of CTAB addition on the crystallinity and the crystalline orientation of the BHJ film. As shown in Figures 4(a) and 4(b), both P3HT:$PC_{60}BM$ BHJ films without and with CTAB yielded well-developed Bragg diffraction peaks in the q_z direction, which corresponds to the lamellar crystalline stacking of P3HT, and a distinct π-π stacking peak in the q_{xy} direction, which corresponds to the edge-on orientation of P3HT. In addition, the Bragg diffraction peak position stayed constant regardless of the addition of CTAB. However, pole figure analyses allowed us to see important differences between the two films in terms of crystalline orientation. The pole figures presented in Figure 4(c) were normalized to the (200) scattered intensity for each film to facilitate comparison. For the pole figure analysis, we analyzed the distribution of the (200) orientation to avoid the surface

scattering effects resulting from the substrate. The pristine BHJ film without CTAB showed a preferential edge-on orientation, with the most of the crystallites oriented at a polar angle of 20°, while the BHJ film with CTAB possessed a broader range of orientations, up to 30°. We also calculated the relative degree of crystallinity (rDoC) by integration of the relative population distribution while considering factors such as X-ray exposure time, beam domain size, and sample thickness, and we determined rDoC values of 1.0 and 0.928 for the CTAB-free and CTAB-added films, respectively. Together with morphological and optical observations, these structural analyses indicate that the addition of CTAB as a surfactant within the P3HT:$PC_{60}BM$ BHJ successfully suppressed donor-donor interaction and facilitated the intermixing of the donor and the acceptor, resulting in a well-mixed, interpenetrating nanomorphology. The estimated crystalline structures are schematically described in the insets of Figure 4 (a) and (b).

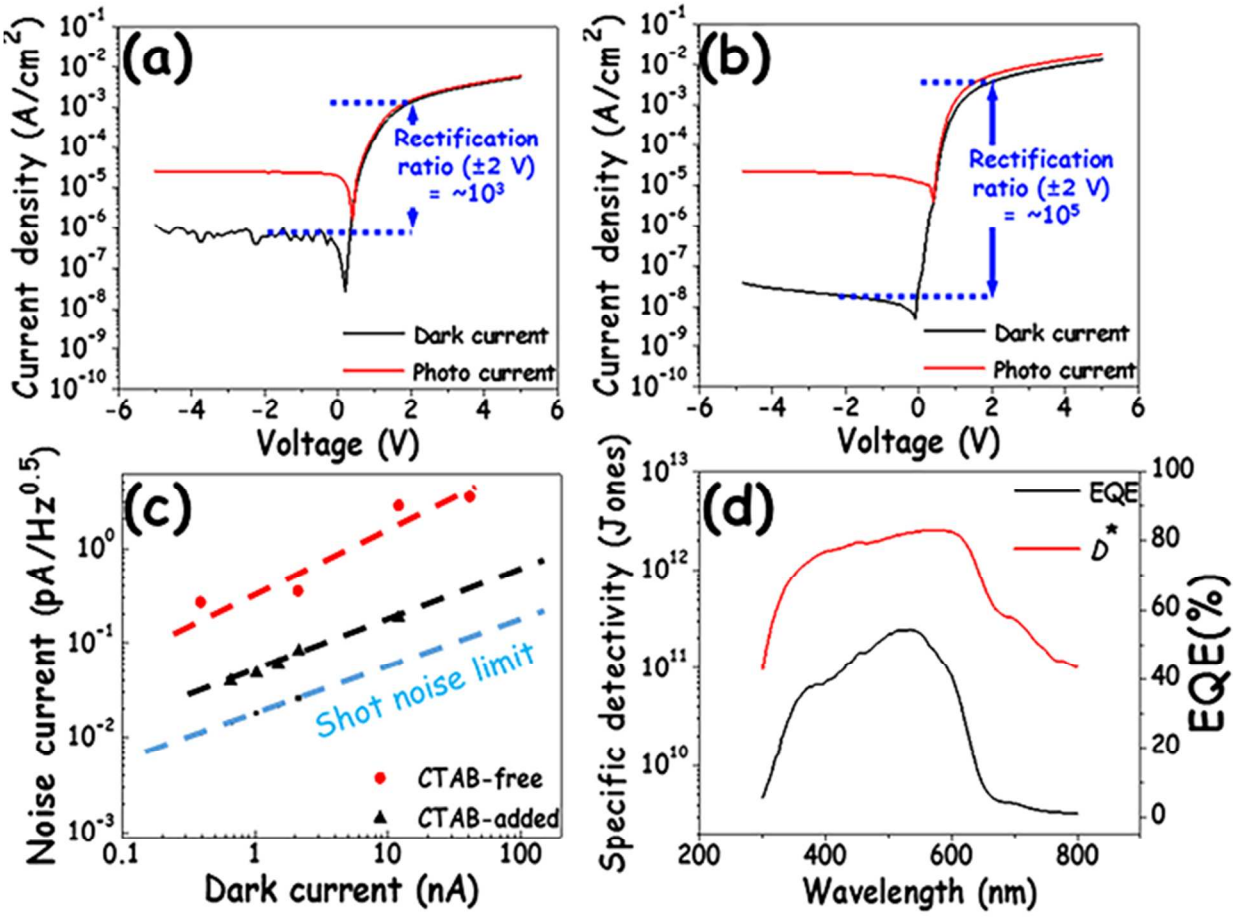

Figure 5 The dark and photo (47 μW/cm^2 and 520 nm) current density−voltage (*J*−*V*) characteristics for (a) CTAB-free photodiode and (b) CTAB-added photodiode, (c) the measured noise current of both photodiode together with theoretically calculated shot noise limit of CTAB-added photodiode, (d) specific detectivity and external quantum efficiency spectra of the optimized CTAB-added photodiode structures measured at −1 V.

Figures 5(a) and 5(b) compare the dark and illuminated (520 nm, 47 μW/cm^2) *J*-*V* curves of the inverted diode without and with CTAB, respectively. In the case of the CTAB-free photodiode (Figure 5(a)), because of the non-rectifying electrode combination, the rectification ratio (±2 V) of the dark *J*-*V* curve is low, ~10^3. In strongly contrast, in the case of the CTAB-added photodiode, a high rectification ratio (±2 V) of ~10^5 was achieved because of the shift in the ITO work function. As shown in Figure 5(c), the measured noise current levels of two devices are compared. The CTAB-added photodiode closely follows its shot noise limit, with an order of

magnitude lower values compared to CTAB-free photodiode, implying an ideal diode operation mechanism in the CTAB-added photodiode under the reverse saturation mode of the photodiode. Based on the obtained EQE and noise current level, *D** spectra were calculated, and these are summarized in Figure 5(d). When operating at room temperature, the CTAB-added photodiode exhibited a spectral response from 300 to 800 nm, with detectivity greater than 10^{12} Jones at a wavelength of 350–650 nm, corresponding to the entire visible range, comparable to other recently reported high performance OPDs. [26~28]

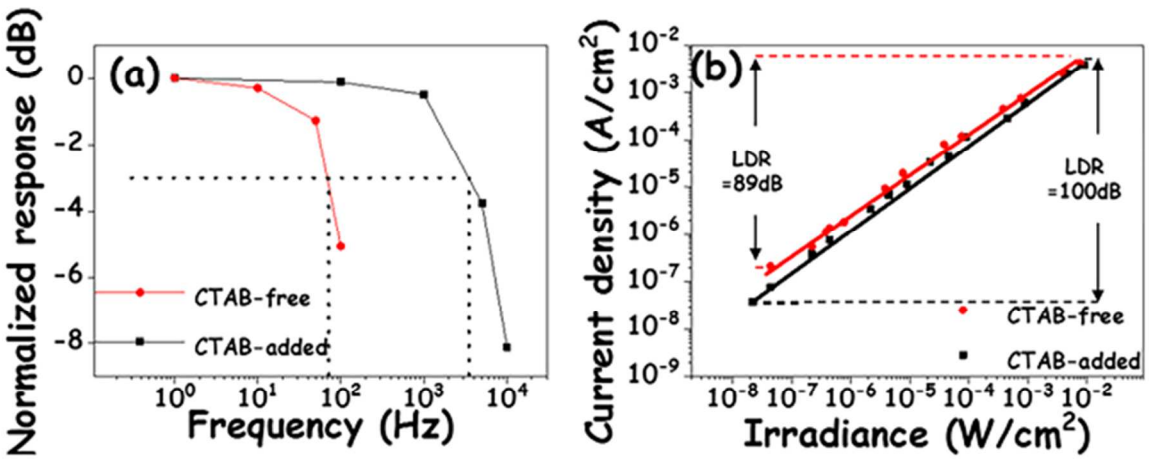

Figure 6 (a) The Bode plot under the monochromated light (520 nm) illumination of 0.9 mW/cm^2 at −1 V. The −3 dB frequency points are specified with dashed lines. (b) The linear dynamic range (LDR) for the optimized photodiode measured at −1 V with 520 nm of illuminated light wavelength.

We also measured the frequency response to characterize the bandwidth of our photodiode. The bandwidth is defined as the frequency of the input light modulation at which the photoresponse is −3 dB (~70.8 %) lower than the continuous wave response. The photoresponse of the photodiode was measured as a function of the modulation frequency of input light at an irradiance of 0.9 mW/cm^2, wavelength (λ) of 520 nm, and a reverse bias of −1 V, as shown in Figure 6(a). The −3 dB frequency values were found to be 70 Hz and 4 kHz for CTAB-free and

CTAB-added photodiodes, respectively. Theoretically, the −3-dB bandwidth can be expressed by:[21]

$$\frac{1}{f_{-3dB}^2} = \frac{1}{f_t^2} + \frac{1}{f_{RC}^2}$$

where f_t and f_{RC} are the carrier transit time-limited and RC-limited bandwidths, respectively. f_t and f_{RC} can be calculated as $f_t = 3.5/(2\pi t_{tr})$ and $f_{RC} = 1/(2\pi RC)$, respectively. t_{tr} is the carrier transit time, R is the total series resistance and C is the capacitance. From dark *J-V* characteristics, R values were determined as 612 Ω cm^2 and 481 Ω cm^2 for CTAB-free photodiode and for CTAB-added photodiode, respectively. Based on the capacitance values of the active layer ~3.8 nF/cm^2, we determined f_{RC} values as 68.5 kHz and 87.2 kHz for the case of CTAB-free and CTAB-added, respectively, Therefore, it can be assumed that the measured f_{-3dB} is fully dependent on the transit time-limited frequency in both cases, with corresponding t_{tr} values of 8 ms and 139 μs for CTAB-free and CTAB-added photodiodes, respectively. The dramatically shortened transit time of CTAB-added photodiode can be attributed to the formation of percolation pathway of both hole and electron as well as much smoother morphology, enabled by better miscibility between donor and acceptor. In addition, we measured the linear dynamic range (LDR), which is the range in dB of incident light irradiance over which the responsivity is constant. A plot of the photocurrent versus input light power (irradiance) at 520 nm for the pristine CTAB-free and CTAB-added photodiodes is shown in Figure 6(b). The photocurrent was found to increase linearly with irradiance up to ~10^{-2} W/cm^2, and the minimum detectable light intensities in our system were 4.4 × 10^{-8} W/cm^2 for the CTAB-free devices and 2.2× 10^{-8} W/cm^2 for the CTAB-added devices. Theoretically, the LDR can be calculated with the formula:[29]

$$\mathbf{LDR} = \mathbf{20}\log\left(\frac{J_{max}}{J_{min}}\right)$$

where J_{max} and J_{min} are the maximum and minimum detectable current densities. With this relation, the LDR of the CTAB-free devices and the CTAB-added devices is calculated as 89 dB and 100 dB, respectively. Moreover, the irradiance dependence of the photocurrent can be linearly fitted with a slope of 0.80 for the CTAB-free devices and 0.88 for the CTAB-added devices. This close to unity in slope values shows evidence that addition of CTAB results in a reduction of charge recombination, consistent with previous experimental results.[30]

Conclusion

In summary, we have reported a new and facile method to realize high quantum efficiency and low noise current in an inverted photodiode. We have demonstrated the preferential adsorption of ammonium cations, as CTAB, onto the ITO surface during the solidification of a deposited ternary solution consisting of P3HT:$PC_{60}BM$:CTAB, which successfully tuned the work function of the ITO surface to 4.55 eV, adequate for anode applications in the inverted photodiode. In other words, the addition of CTAB made it possible to fabricate photodiodes with an ITO/P3HT:$PC_{60}BM$:CTAB/MoO_3/Ag diode structure as an inverted photodiode, avoiding the need for a ZnO/TiO_2 interlayer, whose fabrication requires the use of toxic components and high processing temperature. We found that, on adding CTAB, the active layer underwent several important changes: 1) the surface energies of pristine P3HT and $PC_{60}BM$ became similar, and 2) the DSC thermal profile and the UV-Vis absorption spectrum became featureless, all of which support the enhanced inter-miscibility of P3HT and $PC_{60}BM$ on the addition of CTAB. GIXD studies revealed that the crystallinity of P3HT, both regarding crystallinity and crystalline orientation, was reduced. As a result, the optimized inverted photodiode showed a high detectivity of 2.5×10^{12} Jones with a reasonably low noise current level of 4×10^{-1} $pA/Hz^{0.5}$. In addition, a high bandwidth of 4 kHz and high LDR of 100 dB were observed, which can be comparable to those of inorganic photodiodes.

Acknowledgement

This research was supported by the Space Core Technology Development Program and Basic Science Research Program through the National Research Foundation of Korea (NRF) funded

by the Ministry of Education (Grant Number: NRF-2014M1A3A3A02034707 and NRF-2015R1C1A1A02037219)

AUTHOR INFORMATION

Corresponding Author

D. S. Chung, *E-mail: dchung@dgist.ac.kr

References

(1) Pierre, A.; Gaikwad, A.; Arias, A. C. Charge-integrating organic heterojunction phototransistors for wide-dynamic-range image sensors. *Nat. Photon.* **2017***, 11*, 193-199.

(2) Li, W.; Li, D.; Dong, G.; Duan, L.; Sun, J.; Zhang, D. Wang, L. High-stability organic red-light photodetector for narrowband applications. *Laser Photon. Rev*. **2016**, *10*, 473-480.

(3) Yoon, S.; Ha, J.; Cho, J.; Chung, D. S. Organic Photodiodes: Nonabsorbing Acceptor-Based Planar Heterojunction for Color-Selective and High-Detectivity Polymer Photodiodes. *Adv. Opt. Mater.* **2016**, *4*, 1933-1938.

(4) Baierl, D.; Pancheri, L.; Schmidt, M.; Stoppa, D.; Dalla Betta, G.-F.; Scarpa, G.; Lugli, P. A hybrid CMOS-imager with a solution-processable polymer as photoactive layer. *Nat. Commun*. **2015**, *3*, 1175.

(5) Pierre, A.; Deckman, I.; Lechêne, P. B.; Arias, A. C. High Detectivity All-Printed Organic Photodiodes. *Adv. Mater.* **2015**, *27*, 6411-6417.

(6) Knipp, D.; Herzog, P. G.; Stiebig, H. Stacked amorphous silicon color sensors. *IEEE Trans. Electron. Dev*. **2002**, *49*, 170-176.

(7) Lule, T.; Benthien, S.; Keller, H.; Mutze, F.; Rieve, P.; Seibel, K.; Sommer, M.; Bohm, M. Sensitivity of CMOS based imagers and scaling perspectives. *IEEE Trans. Electron Dev.* **2000**, *47*, 2110-2122.

(8) Konstantatos, G.; Sargent, E. H. Nanostructured materials for photon detection. *Nat. Nanotechnol.* **2010**, *5*, 391-400.

(9) Lee, K. H.; Leem, D. S.; Castrucci, J. S.; Park, K. B.; Bulliard, X.; Kim, K. S.; Park, S. Y. Green-Sensitive Organic Photodetectors with High Sensitivity and Spectral Selectivity Using Subphthalocyanine Derivatives. *ACS Appl. Mater. Interfaces*, **2013**, *5*, 13089-13095.

(10) Ohta, J. *Smart CMOS Image Sensors and Applications*; CRC Press, Boca Raton, FL, USA, **2007**.

(11) Someya, T.; Kato, Y.; Iba, S.; Noguchi, Y.; Sekitani, T.; Kawaguchi, H.; Sakurai, T. Integration of Organic FETs with Organic Photodiodes for a Large Area, Flexible, and Lightweight Sheet Image Scanners. *IEEE Trans. Electron. Dev.* **2005**, 52, 2502-2511.

(12) Ng, T. N.; Wong, W. S.; Chabinyc, M. L.; Sambandan, S.; Street, R. A. Flexible Image Sensor Array with Bulk Heterojunction Organic Photodiode. *Appl. Phys. Lett.* **2008**, 92, 213303.

(13) Falco, A.; Cinà, L.; Scarpa, G.; Lugli, P.; Abdellah, A. Fully-Sprayed and Flexible Organic Photodiodes with Transparent Carbon Nanotube Electrodes. *ACS Appl. Mater. Interfaces*, **2014**, 6, 10593-10601.

(14) Gong, X.; Tong, M.; Xia, Y.; Cai, W.; Moon, J. S.; Cao, Y.; Yu, G.; Shieh, C. -L. Nilsson, B.; Heeger, A. J. High-Detectivity Polymer Photodetectors with Spectral Response from 300 nm to 1450 nm. *Science,* **2009**, 325, 1665-1667.

(15) Armin, A.; Jansen-van Vuuren, R. D.; Kopidakis, N.; Burn, P. L.; Meredith, P. Narrowband Light Detection via Internal Quantum Efficiency Manipulation of Organic Photodiodes. *Nat. Commun*. **2015**, 6, 6343.

(16) Gong, X.; Tong, M. -H.; Park, S. H.; Liu, M.; Jen, A.; Heeger, A. J. Semiconducting Polymer Photodetectors with Electron and Hole Blocking Layers: High Detectivity in the Near-Infrared. *Sensors*, **2010**, 10, 6488-6496.

(17) Valoucha, S.; Hönesa, C.; Kettlitza, S. W.; Christa, N.; Doa, H.; Kleina, M. F. G.; Kaltb, H.; Colsmanna, A.; Lemmer, U. Solution Processed Small Molecule Organic Interfacial Layers for Low Dark Current Polymer Photodiodes. *Org. Electron.* **2012**, 13, 2727-2732.

(18) Ro, H. W.; Downing, J. M.; Engmann, S.; Herzing, A. A.; DeLongchamp, D. M.; Richter, L. J.; Mukherjee, S.; Ade, H.; Abdelsamie, M.; Jagadamma, L. K.; Amassian, A.; Liu, Y.; Yan, H. Morphology Changes Upon Scaling a High-efficiency, Solution-processed Solar Cell. *Energy Environ. Sci.* **2016**, 9, 2835-2846.

(19) Lee, J. H.; Kim, K. M.; Jang, W.; Ahn, S.; Kim, Y. Y.; Park, O. O.; Wang, D. H. Vacuum-process-based Dry Transfer of Active Layer with Solvent Additive for Efficient Organic Photovoltaic Devices. *J. Mater. Chem. C.* **2017**, 5, 1106-1112.

(20) Hoven, C. V.; Dang, X. -D.; Coffin, R. C.; Peet, J.; Nguyen, T. -Q.; Bazan, G. C. Improved Performance of Polymer Bulk Heterojunction Solar Cells Through the Reduction of Phase Separation via Solvent Additives. *Adv. Mater.* **2010**, 22, E63-E66.

(21) Armin, A.; Hambsch, M.; Kim, I. K.; Burn, P. L.; Meredith, P.; Namdas, E. B. Thick Junction Broadband Organic Photodiodes, *Laser. Photon. Rev.* **2014**, 8, 924-932.

(22) Zhou, Y.; Fuentes-Hernandez, C.; Shim, J.; Meyer, J.; Giordano, A. J.; Li, H.; Winget, P.; Papadopoulos, T.; Cheun, H.; Kim, J.; Fenoll, M.; Dindar, A.; Haske, W.; Najafabadi, E.; Khan, T. M.; Sojoudi, H.; Barlow, S.; Graham, S.; Brédas, J. -L.; Marder, S. R.; Kahn, A.; Kippelen, B.

A Universal Method to Produce Low–Work Function Electrodes for Organic Electronics. *Science*, **2012**, 336, 327-332.

(23) Keivanidis, P. E.; Ho, P. K. H.; Friend, R. H.; Greenham, N. C. The Dependence of Device Dark Current on the Active-Layer Morphology of Solution-Processed Organic Photodetectors. *Adv, Funct. Mater.* **2010**, 20, 3895-3903.

(24) Wetzelaer, G. A. H.; Kuik, M.; Lenes, M.; Blom, P. W. M. Origin of the Dark-current Ideality Factor in Polymer:fullerene Bulk Heterojunction Solar Cells. *Appl. Phys. Lett.* **2011**, 99, 153506.

(25) Zhao, J.; Swinnen, A.; Assche, G. V.; Manca, J.; Vanderzande, D.; Mele, B. V. Phase Diagram of P3HT/PCBM Blends and Its Implication for the Stability of Morphology. *J. Phys. Chem. B.* **2009**, 113, 1587-1591.

(26) Dong, R.; Bi, C.; Dong, Q.; Guo, F.; Yuan, Y.; Fang, Y.; Xiao Z.; Huang, J. An Ultraviolet-to-NIR Broad Spectral Nanocomposite Photodetector with Gain. *Advanced Optical Materials*, **2014**, *2*(6), 549-554.

(27) Azzellino, G.; Grimoldi, A.; Binda, M.; Caironi, M.; Natali, D.; Sampietro, M. Fully Inkjet-Printed Organic Photodetectors with High Quantum Yield. *Advanced Materials*, **2013**, *25*(47), 6829-6833.

(28) Wu, S.; Xiao, B.; Zhao, B.; He, Z.; Wu, H.; Cao, Y. High Sensitivity Polymer Visible-Near Infrared Photodetectors via an Inverted Device Structure and Manipulation of Injection Barrier Height. *Small*, **2016**, *12*(25), 3374-3380.

(29) Jansen-van Vuuren, R. D.; Armin, A.; Pandey, A. K.; Burn, P. L.; Meredith, P. Organic Photodiodes: The Future of Full Color Detection and Image Sensing. *Adv. Mater.* **2016**, 28, 4766-4802.

(30) Yoon, S.; Cho, J.; Sim, K. M.; Ha, J.; Chung, D. S. Low Dark Current Inverted Organic Photodiodes Using Anionic Polyelectrolyte As a Cathode Interlayer. *Appl. Phys. Lett.* **2017**, 110, 083301.

Table of Contents

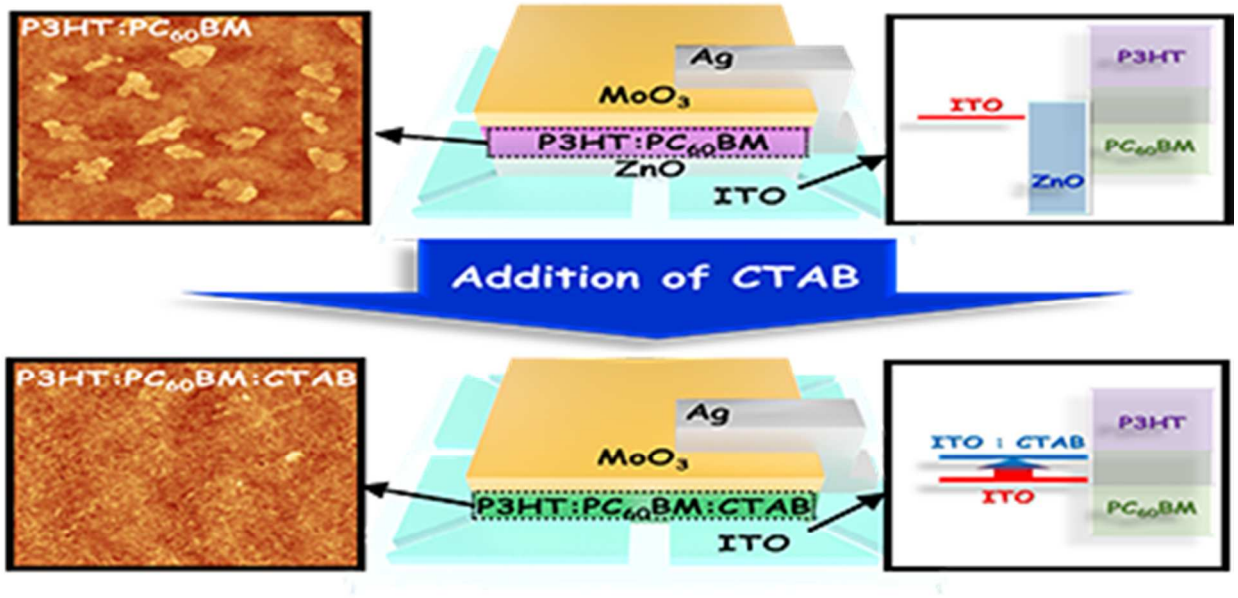

This study proposes A new and facile photodiode fabrication strategy for inverted organic photodiodes by adding small amount of surfactant. This new fabrication method successfully tunes work function of ITO and promote miscibility between the donor and the acceptor. Owing to the synergetic effects of the surfactant additive showed outstanding photodetector characteristics.